

Horizon Detection for Mars Surface Operations

Steven Lu
Jet Propulsion Laboratory
California Institute of Technology
4800 Oak Grove Drive, Pasadena, CA 91109
818-354-7760
You.Lu@jpl.nasa.gov

Stephanie Lynn Oij
Jet Propulsion Laboratory
California Institute of Technology
4800 Oak Grove Drive, Pasadena, CA 91109
818-354-6981
Stephanie.L.Oij@jpl.nasa.gov

Abstract—A new image processing method for automated horizon detection is presented in this paper. This method was developed for the Mars Exploration Rovers mission’s surface operations to aid in determining orbiter visibility periods for downlink data, and is now being considered for all Mars surface missions and for a variety of applications. Starting with images received from Mars rovers or landers, the horizon pixel location is found by (1) obtaining the gradient images using the Sobel operator, (2) calculating the preliminary horizon locations by optimizing the maximum difference between sky and ground regions in the gradient domain, and (3) applying a multi-variable thresholding method. The results are analyzed using a variety of images from the Mars rovers, as an example one dataset’s results were categorized as 94.2% Good, 4.11% Okay, and 1.65% Poor. The pixel location corresponding to the found horizon in an image is converted to azimuth and elevation values using the camera model. The elevation of the terrain surrounding the rover or lander directly affects the duration orbiters are visible for downlink data volume, and when the sun is visible for image quality or solar energy consumption. Having an automated process to detect the elevation of the terrain allows the operation team to better predict the outcome of the plan, reducing health and safety risks and allowing new operational limits to be defined.

last plan, and if all the necessary data has been received in order to plan certain observations or activities on the current sol, or next few sols. The plan contains everything the rover will execute including drives, arm activities, science observations, imaging, and when to communicate with orbiters and Earth.

The amount of data we receive from the rover can limit what observations and activities can be planned on subsequent sols. For example, if the expected imaging is not received, there may not be enough information to plan a drive or activities with the rover’s robotic arm. It is important to know how much data volume will be received so science and engineering teams know how to prioritize activities and the order in which the data will be received.

Most commonly, data is received from the rover via a relay through a Mars orbiter. The duration the orbiter is visible by the rover directly affects the data volume the orbiter receives, therefore the data volume Earth receives. One major impact on the orbiter’s visibility is the local topography surrounding the rover. If the rover is near high terrain, this can occlude communication with the orbiter for some period of time, shrinking the downlink data volume.

In order to mitigate unpredictable downlink data volumes due to surrounding topography, the local horizon is determined using the methods described in this paper. With these methods, the rover operations team can generate more accurate estimates for downlink data volume with little manual effort on a tactical timeline.

Horizon detection technologies in the image processing domain have been broadly studied and used for different purposes. In [3], a robust horizon detection method is proposed to aid in determining attitude for unmanned aerial vehicles. The possible horizon profiles are extracted from red, green, and blue bands of a RGB image, and then a adaptive threshold algorithm is applied to find the final horizon profile. In [1], a principal component analysis based method is proposed to detect horizon profile for autonomous ground robot navigation.

The majority of the past work and research was conducted using images or videos taken on Earth. An important factor that must be considered is that there are no trees, buildings, or other man-made objects on Martian surface. If these objects are in images taken on Earth and they occupy entire columns, then these columns need to be excluded from detected horizon profiles. This additional step is usually computationally intensive. In [1], a method using K-means clustering and Mahalanobis distance is discussed for detecting and removing these columns in images. As a comparison to the images taken on Mars, there is no need to perform this step.

Often images taken on the Martian surface contain terrain

TABLE OF CONTENTS

1. INTRODUCTION.....	1
2. METHODS	2
3. RESULTS	5
4. CONCLUSION	6
ACKNOWLEDGMENTS	8
REFERENCES	8
BIOGRAPHY	8

1. INTRODUCTION

The Opportunity rover is approaching its 13th year of operations on Mars and continues to collect valuable science data, revealing clues about Mars’ past. The Opportunity rover along with the identical rover, Spirit, makes up the Mars Exploration Rover Project. These two rovers landed on Mars in 2004, with the goal of learning about past water activities, the composition of the surface, and how the terrain was shaped on Mars. The horizon detection methods discussed in this paper were developed for the Opportunity rover, however, they are applicable to any Mars lander or rover.

Mars rover operations planning begins by receiving a downlink from Mars, containing data regarding the current state of the rover and any science or engineering observations that occurred on the previous sol, or Martian day. The downlink is analyzed to determine if everything went as expected in the

far away from the rover or lander, where there is no distinct separation between sky and ground regions. These regions are defined as weak horizons. The lack of distinct separation is often caused by atmospheric dust, which causes distant objects to be less distinct. An example of an image containing weak horizon is shown in Figure 1(b). The characteristics of weak horizon in Mars images is similar to the horizon seen in marine images or the horizon seen by unmanned aerial vehicles at high altitude. Five different algorithms are proposed and compared in [4] to specifically address the issue of detecting horizons where there is no distinct separation between sky and ocean regions; a method of optimization using covariance matrix and eigenvectors is proposed in [2] to detect weak horizons for unmanned aerial vehicles. Sometimes the actual horizon in images taken by the Opportunity rover contain not only a weak horizon, but also a strong horizon with a distinct separation between the sky and ground regions. An example of an image that contains both weak and strong horizons is shown in Figure 1(a).

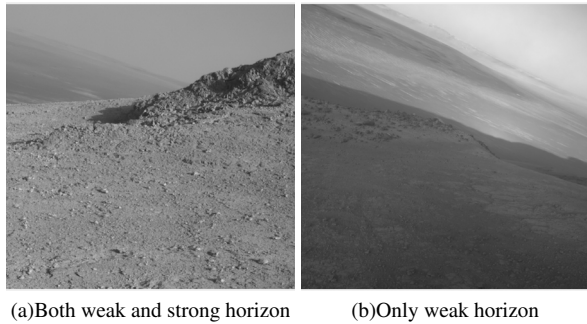


Figure 1. Example of weak and strong horizons.

In order to resolve these issues, we propose a gradient-based multi-thresholding horizon detection method. This paper is organized into several sections to describe these methods. In Section 2, the detailed algorithms are discussed and given in pseudo-code. The performance of the proposed method is analyzed in Section 3. Statistics and example results are provided in Section 3 as well. Finally, conclusions for the proposed method are drawn in Section 4.

2. METHODS

Image Preprocessing

The proposed algorithm to find the horizon profile requires a grey scale image without any color information. If the input image is color, it is converted to grey scale prior to processing. Additionally, before applying the horizon algorithm, the salt-and-pepper noise is blended in the image. This salt-and-pepper noise presents itself as sparsely occurring white and black pixels and affects the detected horizon profile. Applying a median filter in the spatial domain reduces this salt-and-pepper noise in the input image. Note that the kernel size of the median filter depends on the size of the noise, so it needs to be set accordingly.

Gradient Image Calculation

Once the image is grey scale with the salt-and-pepper noise removed, the gradient magnitude and the gradient direction images are calculated using the Sobel operator. The horizontal and vertical kernels of the Sobel operator are designed to respond maximally to edges running horizontally and vertically, respectively [7]. The horizontal and vertical kernels of

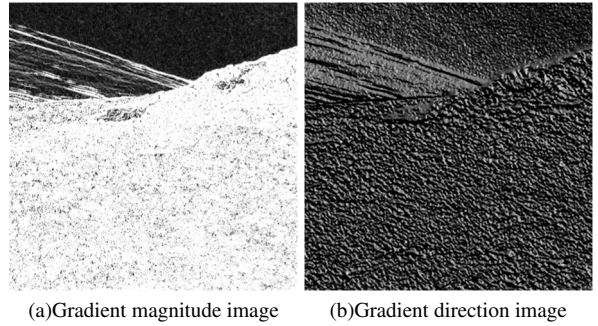


Figure 2. Gradient magnitude and direction images.

the Sobel operator are defined as

$$h = \begin{bmatrix} -1 & 0 & 1 \\ -2 & 0 & 2 \\ -1 & 0 & 1 \end{bmatrix} \quad (1)$$

$$v = \begin{bmatrix} 1 & 2 & 1 \\ 0 & 0 & 0 \\ -1 & -2 & -1 \end{bmatrix} \quad (2)$$

where h is the horizontal component and v is the vertical component. The horizontal gradient image G_x and the vertical gradient image G_y are calculated by the convolution of the kernel and the image.

$$G_x = I(x, y) * h \quad (3)$$

$$G_y = I(x, y) * v \quad (4)$$

where I is the grey scale image. The gradient magnitude and direction images are then obtained by combining G_x and G_y with the equations

$$G_{mag} = \sqrt{G_x^2 + G_y^2} \quad (5)$$

$$G_{dir} = \arctan \frac{G_y}{G_x} \quad (6)$$

where G_{mag} is the gradient magnitude image as shown in Figure 2(a), and G_{dir} is the gradient direction image, which measured in degrees, as shown in Figure 2(b). The gradient magnitude and direction images are normalized for viewing purposes.

Preliminary horizon detection

The optimization method used to find the preliminary horizon profile in gradient domain is inspired by the covariance matrix based optimization approaches in intensity domain, described in [1] and [3]. Due to the characteristics of the images acquired by the Opportunity rover, the optimization method of finding the horizon profile in the gradient domain is not always successful. Opportunity's images often contain weak horizon regions due to far away terrain in the image. In these regions, the intensity level of the horizon is close to the intensity level of the sky region causing the horizon profile information to be found using this method to be inconsistent. The weak horizon regions in the gradient magnitude image are represented as weak edges. Note that these weak edges are still significantly stronger than the edges in sky regions caused by salt-and-pepper noise. The method to find the preliminary horizon profile begins by defining the horizon

profile function $P(x)$:

$$1 \leq P(x) \leq H, 1 \leq x \leq W \quad (7)$$

where H and W are the height and width of the image respectively, and $P(x)$ determines the horizon profile position for the x^{th} column. To calculate the gradient magnitude of sky and ground regions, the regions are defined with the following equations:

$$G_{mag}^s = \{(x, y) | 1 \leq x \leq W, 1 \leq y \leq P(x)\} \quad (8)$$

$$G_{mag}^g = \{(x, y) | 1 \leq x \leq W, P(x) < y \leq H\} \quad (9)$$

The gradient magnitude image contains changes in intensity of the original image. Large changes in the gradient magnitude image correspond to a busier activity scene in the original image, and small changes in the gradient magnitude image correspond to a smoother activity scene in the original image. Therefore, the gradient magnitude image is used to measure the busyness of original image. With the help of equations (8) and (9), the gradient magnitude image is logically divided into the sky gradient magnitude and the ground gradient magnitude. The busyness levels, denoted as B_{avg}^s and B_{avg}^g for the sky gradient magnitude and the ground magnitude regions, are then calculated by finding the average magnitude values, as shown in the following equations.

$$B_{avg}^s = \frac{\sum_{i=1}^x \sum_{j=1}^{P(x)} G_{mag}^s(i, j)}{\sum_{i=1}^x P(x)} \quad (10)$$

$$B_{avg}^g = \frac{\sum_{i=1}^x \sum_{j=P(x)+1}^H G_{mag}^g(i, j)}{\sum_{i=1}^x (H - P(x))} \quad (11)$$

Note that G_{mag}^s and G_{mag}^g are the same size as the original image. The ground region of G_{mag}^s and the sky region of G_{mag}^g are filled with zeros. The preliminary horizon profile is determined by finding the function $P(x)$ that causes the greatest difference between B_{avg}^s and B_{avg}^g , as shown in Algorithm 1. Having a constant threshold value t_{strong}

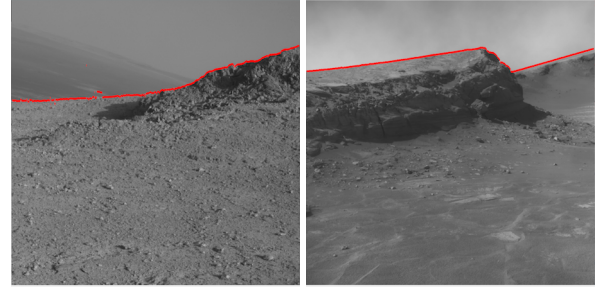
Algorithm 1 Calculate horizon profile function $P(x)$

```

1: procedure CAL_TMP_HORIZON_PROFILE( $t_{strong}$ )
2:   for  $x = 0$  to  $img\_width - 1$  do
3:      $P(x) = img\_height - 1$ 
4:     for  $y = 0$  to  $img\_height - 1$  do
5:       if  $G_{mag}(y, x) > t_{strong}$  then
6:          $P(x) = y$ 
7:       break
8:     end if
9:   end for
10:  end for
11:  return  $P(x)$ 
12: end procedure

```

allows the horizon profile function $P(x)$, and therefore the average magnitude values of sky and ground regions in (10) and (11), to be easily calculated. However, the constant threshold value is not a constant number and is optimized by searching in a 1 dimensional space. Once the optimal t_{strong} is found, the preliminary horizon profile function



(a)Preliminary horizon profile (b)Preliminary horizon profile

Figure 3. Preliminary horizon detection results (The preliminary detected profiles are marked in red).

$P_{pre}(x)$ is found by using the algorithm introduced in Algorithm 2. The inputs t_{min} , t_{max} , and $t_{increment}$ are user-defined parameters. These parameter values are set based on image statistics, such as how many bits are used to represent a pixel value and what level of noise is presented in the image. Changing the t_{min} and t_{max} values do not alter the resulting profile function, but only change the computation time. The images acquired by the Opportunity rover are 12-bit. By balancing the detection accuracy and computational complexity, t_{min} is set to 200, t_{max} is set to 1000, and $t_{increment}$ is set to 50.

Algorithm 2 Calculate preliminary horizon profile function

$P_{pre}(x)$

```

1: procedure CAL_PRELIM_HORIZON_PROFILE( $t_{min}$ ,
    $t_{max}$ ,  $t_{increment}$ )
2:    $n = \frac{t_{max} - t_{min}}{t_{increment}}$ 
3:   for  $k = 1$  to  $n$  do
4:      $J_{max} = 0$ 
5:      $t = t_{min} + \frac{t_{max} - t_{min}}{n - 1} \times (k - 1)$ 
6:      $P = cal\_tmp\_horizon\_profile(t)$ 
7:     compute  $B_{avg}^s$  based on equation (10)
8:     compute  $B_{avg}^g$  based on equation (11)
9:      $J = B_{avg}^g - B_{avg}^s$ 
10:    if  $J > J_{max}$  then
11:       $J_{max} = J$ 
12:       $P_{pre} = P$ 
13:    end if
14:  end for
15:  return  $P_{pre}$ 
16: end procedure

```

The preliminary horizon profile only shows the most obvious edges, with some of these edges containing the true horizon profile and some not. In general, if there is no weak horizon presented in the image and the noise in the image is within a reasonable level, then the preliminary horizon profile should be accurately detected as shown in Figure 3(b). However, if weak horizon is presented in the image, then the preliminary horizon profile will be discontinuous as shown in Figure3(a).

Weak horizon detection

Since the intensity of the weak horizon is similar to the intensity of the sky, the corresponding edges in gradient magnitude image are weak. The weak horizon profile is detected by searching upwards in every column of the preliminary horizon profile. It is quite often the case that the preliminary horizon profile contains outliers and regions of false horizon. In order to improve the accuracy of detecting the weak horizon profile, a standard median filter described in [10] is applied to the preliminary horizon profile function $P_{pre}(x)$ to set the positions of the outliers to the median positions of its neighbors.

After the outliers have been refined, the preliminary horizon profile will be in a state where some of the columns contain the actual horizon profile and some columns still contain false horizon lower than the true horizon. With the preliminary horizon profile function, the sky region G_{mag}^s is refined as:

$$G_{mag}^s = \{(x, y) | 1 \leq x \leq W, 1 \leq y \leq P_{pre}(x)\} \quad (12)$$

In order to study the G_{mag}^s region to find if a weak horizon is present, a search process from the refined preliminary horizon profile to the upper boundary of the gradient magnitude image is performed. The process for finding the weak horizon profile function $P_{weak}(x)$ is provided in Algorithm 3 and 4. When clouds occur on Mars, they are quite thin so they typically do not interfere with the weak horizon detection.

Algorithm 3 Calculate weak horizon profile $P_{weak}(x)$

```

1: procedure CAL_WEAK_HORIZON( $t_{weak}$ )
2:   for  $x = 1$  to  $W$  do
3:     for  $y = P_{pre}(x)$  to 1 do
4:       if  $G_{mag}^s > t_{weak}$  then
5:         if  $is\_pattern\_exist(x, y)$  then
6:            $P_{weak}(x) = y$ 
7:         end if
8:       end if
9:     end for
10:  end for
11:  return  $P_{weak}(x)$ 
12: end procedure

```

In Algorithm 3, a threshold value t_{weak} is introduced to calculate the weak horizon profile $P_{weak}(x)$. Its value is estimated based on the similarity between the intensity of the weak terrain region and the intensity of the sky region. For the Opportunity rover's images, the value of t_{weak} is set to 50. Algorithm 4 is used to determine the existence of a horizon profile in a square area in the gradient direction image. Once a position is marked as suspicious weak horizon in Algorithm 3, it is further examined in Algorithm 4. If $\frac{1}{3}$ of the gradient direction values within the square are close to the direction of suspicious weak horizon, then the suspicious weak horizon is classified as weak horizon. Then $P_{weak}(x)$ and $P_{pre}(x)$ are merged into the combined horizon profile function $P_{combined}(x)$ using Algorithm 5.

False horizon removal

The previous steps are applied on all input images regardless of the image content. However, the input images may contain no-sky regions or partial-sky regions. If the input images

Algorithm 4 Determine the existence of horizon pattern in gradient direction image

```

1: procedure IS_PATTERN_EXIST( $x, y$ )
2:    $box\_size = 20$ 
3:    $counter = 0$ 
4:    $interval = 10$ 
5:   for  $i = y - box\_size$  to  $y + box\_size$  do
6:     for  $j = x - box\_size$  to  $x + box\_size$  do
7:       if  $G_{dir}(y, x) - interval \leq G_{dir}(i, j) \leq$ 
8:          $G_{dir}(y, x) + interval$  then
9:          $counter++$ 
10:      end if
11:    end for
12:  end for
13:  if  $counter > \frac{(box\_size * 2 + 1)^2}{3}$  then
14:    return TRUE
15:  else
16:    return FALSE
17:  end if
18: end procedure

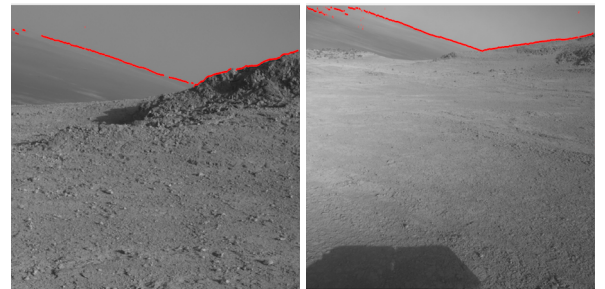
```

Algorithm 5 Calculate $P_{combined}(x)$ by merging $P_{pre}(x)$ and $P_{weak}(x)$

```

1: procedure MERGE
2:   for  $x = 1$  to  $W$  do
3:     if  $P_{weak}(x) \leq P_{pre}(x)$  then
4:        $P_{combined}(x) = P_{weak}(x)$ 
5:     else
6:        $P_{combined}(x) = P_{pre}(x)$ 
7:     end if
8:   end for
9:   return  $P_{combined}(x)$ 
10: end procedure

```



(a) Weak horizon all sky (b) Weak horizon partial sky

Figure 4. Weak horizon detection results.

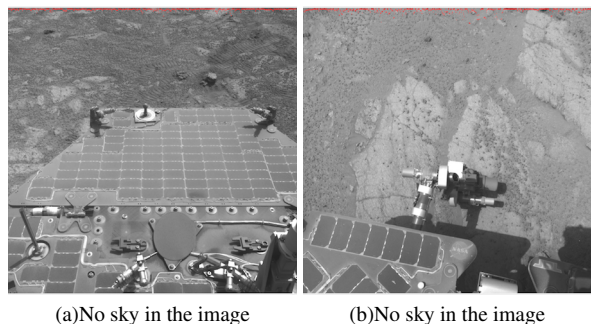


Figure 5. Weak horizon detection results when there is no sky in the images.

contain no-sky regions or partial-sky regions, the resultant $P_{combined}(x)$ will contain outliers or a false horizon profile. The outliers or the false horizon profile for the no-sky columns need to be removed. Figure 4 and Figure 5 show images with $P_{combined}(x)$ overlaid on top. In Figure 4(b), a few columns on the left side of the image do not contain any sky, and in Figure 5, both images contain no sky at all. Using the previous proposed method, a false horizon profile is detected. From the example shown in the analysis conducted, the false horizon profile in $P_{combined}(x)$ always appears to be discontinuous and very close to the upper boundary of the image. To test discontinuities in $P_{combined}(x)$, the absolute difference p_{dif} of $P_{combined}(x)$ is calculated using the equation defined below:

$$p_{dif} = \sum_{x=2}^W |P_{combined}(x) - P_{combined}(x-1)| \quad (13)$$

A large p_{dif} indicates that $P_{combined}(x)$ changes frequently over the columns. In order to test whether $P_{combined}(x)$ is close to the upper boundary of the image, the average position of $P_{combined}(x)$ is calculated as denoted below:

$$p_{avg} = \frac{1}{W} \sum_{x=1}^W P_{combined}(x) \quad (14)$$

A small p_{avg} indicates that $P_{combined}(x)$ is close to the upper boundary of the image. With the help of these two equations, a recursive method of finding final horizon profile P_{final} is given in Algorithm 6. The method `cal_final_horizon` requires six input parameters. The parameters start and end values indicate the range of $P_{combined}(x)$, where the false horizon needs to be removed. In general, these values are set to 0 and the image width, respectively. Parameters `avg_t1`, `avg_t2`, `dif_t1`, `dif_t2` are used to describe the constraints to remove the false horizon, which `avg_t1` and `avg_t2` define the intervals of horizon position for testing p_{avg} , and `dif_t1` and `dif_t2` define the intervals of horizon absolute difference for testing p_{dif} . In practice, `avg_t1` is set to 10, `avg_t2` is set to 30, `dif_t1` is set to 2, and `dif_t2` is set to 20. An example of the final horizon profile overlaid on top of the input image is shown in Figure 6(a). More results are shown in Section 3.

Converting to azimuth and elevation

Each camera on the Opportunity rover has a corresponding camera model, which is a set of numbers and vectors describing the geometry of the camera optics [9]. The camera model is derived from images taken of calibration targets at a fixed

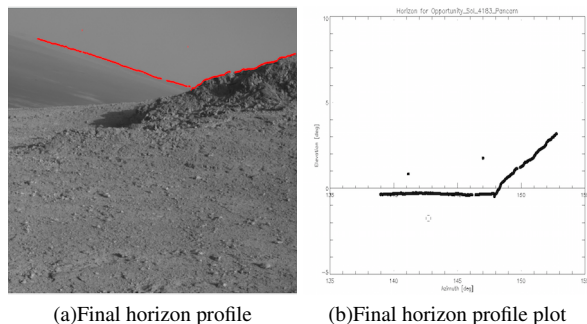


Figure 6. Final horizon profile and its corresponding plot.

azimuth and elevation. A camera model allows each point in space seen by the camera to be traced to a pixel location in the image, as well as each pixel located in the image to be traced to a position in space. Having an accurate camera model is necessary to generate many products used for Mars surface operations.

After using the methods described above to find the horizon profile in an image, the camera model is used to convert these image pixel values to azimuth and elevation values. Having the horizon profile in azimuth and elevation, rather than pixel values, allows the user to better understand the meaning of the horizon profile and makes it directly comparable to the location of orbiters, which are also computed in azimuth and elevation. Figure 6(b) is a plot displaying the elevation of the horizon profile, built by converting each pixel location in the horizon profile to azimuth and elevation values using the camera model. Note that the rover was tilted on a hillside when the image was captured; consequently, the weak horizon appears on an angle in the image. The weak horizon is actually horizontal, as reflected in the plot. The method of finding the azimuth and elevation values of the horizon using the camera model considers the rover's tilt, therefore providing accurate horizon information.

3. RESULTS

The testing dataset consists of 243 16-bit, grey scale images acquired by the Opportunity rover between sols 1 and 4320. Most commonly in operations, the input images used to find the horizon profile are taken with the navigation cameras (navcam) [9], therefore the majority of the images in the dataset are navcam images. In order to test the precision of the proposed method with the other cameras on the Opportunity rover, a small number of the images acquired by the panoramic camera (pancam) and front hazard avoidance camera (front hazcam) [9] are also included in the dataset. As a result the testing dataset contains 223 navcam images, 10 pancam images, and 10 front hazcam images. All of the images in the testing dataset are radiometrically corrected to remove the effects of exposure time and temperature[8].

For validation purposes, the final horizon profile is plotted on top of the input image in order to visually determine the accuracy of the detected horizon profiles. Examples are shown in Figure 3. The horizon profiles are examined manually, and then classified into three categories: "Good", "Okay", and "Poor". If the detected horizon profile covers more than 95% of the actual horizon in the image, then it is classified as "Good"; if the coverage is between 80% and

Algorithm 6 Calculate final horizon profile $P_{final}(x)$

```
1: procedure CAL_FINAL_HORIZON(start, end, avg_t1,
   avg_t2, dif_t1, dif_t2)
2:    $W = end - start$ 
3:   calculate  $p_{dif}$  using equation (13)
4:   calculate  $p_{avg}$  using equation (14)
5:   if  $p_{avg} \leq avg\_t1$  or ( $p_{avg} \leq avg\_t2$  and  $p_{dif} \geq$ 
   dif_t1) or  $p_{dif} \geq dif\_t2$  then
6:     for  $x = start$  to  $end$  do
7:        $P_{final}(x) = -1$ 
8:     end for
9:   else if  $p_{avg} > avg\_t2$  and  $p_{dif} < dif\_t1$  then
10:    for  $x = start$  to  $end$  do
11:       $P_{final}(x) = P_{combined}(x)$ 
12:    end for
13:   else
14:     if  $end = start + 2$  then
15:       for  $x = start$  to  $end$  do
16:          $P_{final}(x) = -1$ 
17:       end for
18:     else
19:        $mid = \lfloor \frac{end - start}{2} + start \rfloor$ 
20:       cal_final_horizon(start, mid, avg_t1, avg_t2,
   dif_t1, dif_t2)
21:       cal_final_horizon(mid, end, avg_t1, avg_t2,
   dif_t1, dif_t2)
22:     end if
23:   end if
24: end procedure
```

95%, it is classified as "Okay"; and if the coverage is below 80%, it is classified as "Poor".

The proposed method heavily relies on the selection of the threshold values, which varies depending on the conditions when the images were acquired. For operations, a quick-look version of horizon profile is generated using default threshold values in order to generate the product on a tactical timeline. If the quick-look version is unsatisfactory, a revised version is generated by adjusting the threshold values. The horizon profile results are categorized using the default threshold values and the adjusted threshold values, shown in Table 1. Generally in Opportunity rover operations, as long as the detected horizon profile covers more than 80% of the actual horizon, the detected horizon profile is considered acceptable. The percentage of "Good" plus "Okay" using the default threshold values is 88.9%, and the percentage of "Good" plus "Okay" using adjusted threshold values is 98.3%. These statistics indicate that the proposed method meets the operational requirements.

In addition to analyzing the testing dataset as a whole, it was also studied by individual camera and image contents. Table 2 shows the percentage of coverage categories by camera using adjusted threshold values. The proposed method works the best on navcam images, where 98.9% of the detected horizon profiles fall into "Good" category. Opportunity's robotic arm is present in the sky region for most of the

Table 1. Percentages of coverage categories for the entire dataset

	default threshold	adjusted threshold
Good	63.8%	94.2%
Okay	25.1%	4.11%
Poor	11.1%	1.65%

Table 2. Percentages of coverage categories by individual camera using adjusted threshold values

	Navcam	Pancam	Front Hazcam
Good	98.9%	80%	10%
Okay	0.9%	10%	70%
Poor	0.4%	10%	20%

front hazcam images [11], causing disturbance in the horizon profile and thus 70% of the front hazcam images fall into the "Okay" category. Table 3 contains the horizon profile results, separated by the amount of sky in the image. 100% of the time, no horizon profile is found for images containing no horizon. The next best results are found for images containing sky across the entire top of the image. The horizon profile is most difficult to find in images that have both sky and terrain at the top of the image such as in Figure 7(d), 7(e), and 7(f). However, even in these images, the horizon profile statistics are still sufficient to meet operational requirements.

4. CONCLUSION

The horizon profile method proposed in this paper is constructed by considering several existing methods and optimizing the process for the surface of Mars. By combining the relevant steps of horizon detection for unmanned aerial vehicles and autonomous robot navigation on Earth, a horizon detection method is developed for Mars rovers and landers. With this method, the horizon profile found meets the requirements for operational use 98.3% of the time.

Using image processing to determine the location of the horizon surrounding the rover allows the rover operations team to quickly and accurately assess visibility periods for orbiters, and therefore downlink data volumes. Having accurate downlink data volumes at the beginning of the tactical day allows the operations team to prioritize observations and activities and to ensure the necessary data is collected in order to plan the following sol.

While the horizon detection method was developed for determining downlink data volumes, it can also be used to determine when the sun is directly visible by a Mars rover

Table 3. Percentages of coverage categories by completeness of sky regions using adjusted threshold values

	no sky	partial sky	all sky
Good	100%	86.7%	95.6%
Okay	0%	11.1%	2.8%
Poor	0%	2.2%	1.6%

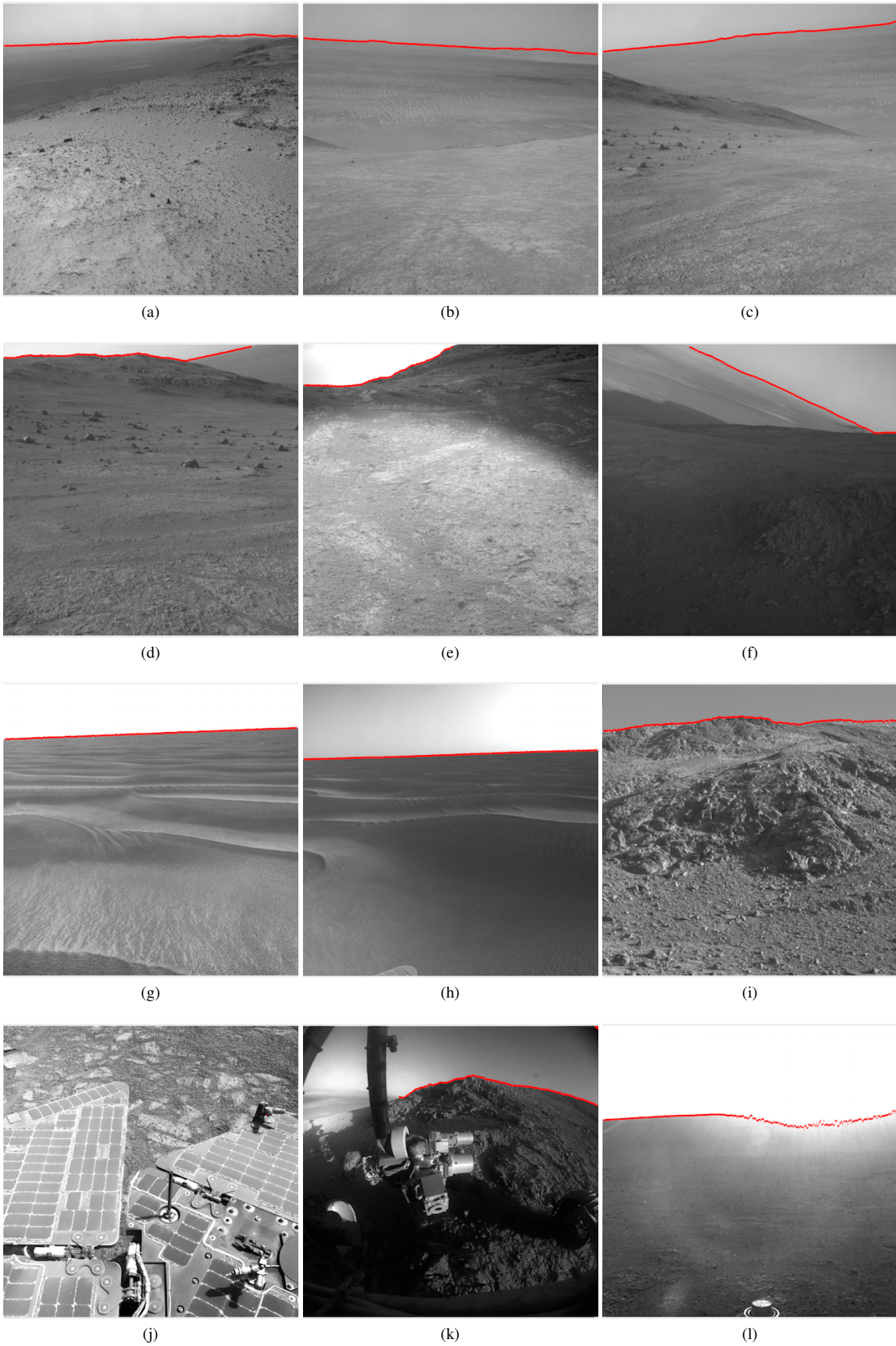


Figure 7. The detected horizon profiles are marked in red. (a)-(c) weak horizon. (d)-(f) partial horizon. (g)-(h) smooth horizon. (i) Pancam. (j) no sky. (k) front Hazcam (l) strong sunlight in the image.

or lander. This will allow the operations teams for solar powered rovers and landers to know when the solar panels are in direct sunlight to accurately generate energy predictions. In addition, knowing if the sun is visible by the rover or lander can support image quality predictions. If the sun is in the image frame, it will wash out the image and may not allow the data products generated by the image to be usable.

At this time, the horizon detection method has been functional in operations for the Opportunity rover for over 100 sols and has proven extremely beneficial. The operations team has been able to predict downlink data volumes more accurate and faster than ever before. The horizon detection method will continue to be used by the Opportunity rover, and is currently being considered for the Curiosity rover and other future Mars missions.

ACKNOWLEDGMENTS

The research described in this paper was conducted at the Jet Propulsion Laboratory, California Institute of Technology, under contract with the National Aeronautics and Space Administration. The authors would like to thank Bob Deen, Amy Chen, Padma Varanasi, and the rest of the Mars Exploration Rovers Operations Team for their help and support with the development of the Horizon Detection Method and its implementation in Rover Operations.

REFERENCES

[1] Yehu Shen and Qicong Wang. Sky Region Detection in a Single Image for Autonomous Ground Robot Navigation. *Int J Adv Robot Syst*, 2013.

[2] Scott M. Ettinger, Michael C. Nechyba, Peter G. Ifju, and Martin Wazak. Vision-Guided Flight Stability and Control for Micro Air Vehicles. *IEEE/RSJ International Conference on Intelligent Robots and Systems*, 2002.

[3] Steven J. Dumble and Peter W. Gibbens. Horizon Profile Detection for Attitude Determination. *J Intell Robot System*, 2012.

[4] Evgeny Gershikov, Tzvika Libe, and Samuel Kosolapov. Horizon Line Detection in Marine Images: Which Method to Choose? *International Journal on Advances in Intelligent Systems*, vol 6 no 1 and 2, 2013.

[5] Yu-Fei Shen, Dean Krusienski, Jiang Li, and Zia-ur Rahman. A Hierarchical Horizon Detection Algorithm. *IEEE Geoscience and Remote Sensing Letters*, 2013.

[6] N. Laungrunthip, A.E. McKinnon, C.D. Churcher, and K. Unsworth. Edge-Based Detection of Sky Regions in Images for Solar Exposure Prediction. *23rd International Conference Image and Vision Computing New Zealand*, 2008.

[7] Raman Maini, and Himanshu Aggarwal. Study and Comparison of Various Image Edge Detection Techniques. *International Journal of Image Processing*, 2009.

[8] Douglass A. Alexander, Robert G. Deen, Paul M. Andres, Payam Zamani, Helen B. Mortensen, Amy C. Chen, Michael K. Cayan, Jeffrey R. Hall, Vadim S. Klochko, Oleg Pariser, Carol L. Stanley, Charles K. Thompson, and Gary M. Yagi. Processing of Mars Exploration Rover Imagery for Science and Operations Planning. *Journal of Geophysical Research*, 111, E02S02, doi:10.1029/2005JE002462, 2006.

[9] J. N. Maki, J. F. Bell III, K. E. Herkenhoff, S. W. Squyres, A. Kiely, M. Klimesh, M. Schwochert, T. Litwin, R. Willson, A. Johnson, M. Maimone, E. Baumgartner, A. Collins, M. Wadsworth, S. T. Elliot, A. Dingizian, D. Brown, E. C. Hagerott, L. Scherr, R. Deen, D. Alexander, and J. Lorre. Mars Exploration Rover Engineer Cameras. *Journal of Geophysical Research*, 108(E12), 8071, doi:10.1029/2003JE002077, 2003.

[10] Sin Hoong Teoh and Haidi Ibrahim. Median Filtering Frameworks for Reducing Impulse Noise from Grayscale Digital Images: A Literature Survey. *International Journal of Future Computer and Communication*, Vol. 1, No. 4, 2012.

[11] Edward Tunstel, Mark Maimone, Ashitey Trebi-Ollennu, Jeng Yen, Rich Petras, and Reg Willson. Mars Exploration Rover Mobility and Robotic Arm Operational Performance. *IEEE International Conference on Systems, Man and Cybernetics, 1807 - 1814 Vol. 2*, DOI: 10.1109/ICSMC.2005.1571410, 2005.

BIOGRAPHY



Steven Lu received his B.S. and M.S. degrees in computer science from Northeastern University in 2009 and California State Polytechnic University at Pomona in 2013, respectively. He is a scientific software engineer at Jet Propulsion Laboratory. His research interests include image processing, computer vision, and machine learning.



Stephanie Lynn Oij graduated from the University of Colorado at Boulder in 2014 with a Bachelors degree in Aerospace Engineering and started at JPL working on the Operational Product Generation Subsystem (OPGS) team for the Mars Exploration Rovers (MER). Since then, she joined the Engineering Cameras (ECAM) and OPGS team on Mars Science Laboratory (MSL), and has helped with instrument planning for Solar Orbiter (SO) and Solar Probe Plus (SPP).